Arabian Journal of Chemistry (2017) **10**, S936–S945

King Saud University

Arabian Journal of Chemistry

www.ksu.edu.sa
www.sciencedirect.com

ORIGINAL ARTICLE

Synthesis, spectroscopic characterization, molecular modeling and eukaryotic DNA degradation of new hydrazone complexes

Ahmed A. El-Asmy *, Ahmed Shabana, Weam Abo El-Maaty, Mohsen M. Mostafa

Chemistry Department, Faculty of Science, Mansoura University, Mansoura, Egypt

Received 4 April 2012; accepted 13 December 2012
Available online 1 February 2013

KEYWORDS

2,5-Hexanedione bis(salicyloylhydrazone);
Spectra;
Antibacterial activity;
Thermal analysis;
ESR;
Molecular modeling

Abstract 2,5-Hexanedione bis(salicyloylhydrazone) [H_4L] formed novel complexes with some transition metal ions. H_4L and its complexes were characterized by elemental analyses, spectral (IR, ^1H NMR, ESR and MS), thermal and magnetic measurements. The complexes have the formulae $[VO(H_2L)]\cdot 2H_2O$, $[Ni(H_2L)]\cdot 3H_2O$, $[Zn(H_2L)]$, $[Ni(H_4L)Cl_2]\cdot 2H_2O$ and $[Cr_2(H_2L)(OAc)_2(OH)_2]$–$\cdot 2H2O$, $[Cu(H_4L)\ (H_2L)(EtOH)_2]\cdot 2H_2O$, $[Co_2(H_2L)(OAc)_2]\cdot H_2O$, $[Mn_2(H_2L)$–$(OH)_2]\cdot H_2O$ $[Cu_2(H_2L)(OAc)_2(H_2O)_6]$, and $[Co_2(H_2L)(H_2O)_4Cl_2]\cdot 2H_2O$. H_4L released its OH or NH protons during the complex formation. Acetate and hydroxo groups bridged the two chromium in $[Cr_2(H_2L)(OAc)_2(OH)_2]\cdot 2H_2O$. The magnetic moments and electronic spectra of all complexes provide: tetrahedral for $[Co_2(H_2L)(OAc)_2]\cdot H_2O$, $[Ni(H_2L)]\cdot 3H_2O$ and $[Zn(H_2L)]$; square-pyramidal for $[VO(H_2L)]\cdot 2H_2O$ and octahedral for the rest. In DMF solution, the bands are shifted to higher energy suggesting a weak interaction with the solvent. The ESR spectra support the mononuclear geometry for $[VO(H_2L)]\cdot 2H_2O$ and $[Cu(H_3L)_2(EtOH)_2]\cdot 2H_2O$. The thermal decomposition of the complexes revealed the outer and inner solvents as well as the end product which in most cases is metal oxide.
© 2013 Production and hosting by Elsevier B.V. on behalf of King Saud University. This is an open access article under the CC BY-NC-ND license (http://creativecommons.org/licenses/by-nc-nd/3.0/).

1. Introduction

Many hydrazones have antimicrobial, antitumor and fungicidal activities due to their ability to form stable chelates with the essential metal ions in which the fungus needs in its metabolism (Petering et al., 1973; Van Giessen et al., 1973; Sharma et al., 2007). Mono- and polynuclear Cu^{2+} complexes serve as models for galactose oxidase and used as an effective oxidant. The redox behavior of the Cu^{2+} model has a special interest in some biological systems (Sevagapandian et al., 2000; Llanguri et al., 2001). Great interest has been focused on the synthesis and structural characterization of hydrazone complexes in order to compare their coordinative behavior with their antimicrobial activities (Thompson et al., 1953). Diacetylmonoxime thiosemicarbazone is effective against vaccine infections in mice by chelating some essential metal ions from the virus (Perrin, 1976). Metal complexes of salicylaldehyde isobutroyl-hydrazone (HSIBuH) and *o*-hydroxy-acetophenone

* Corresponding author. Present address: Chemistry Department, Faculty of Science, Kuwait University, Kuwait. Tel.: +96566734989; fax: +96524816482.
E-mail address: aelasmy@yahoo.com (A.A. El-Asmy).
Peer review under responsibility of King Saud University.

ELSEVIER Production and hosting by Elsevier

http://dx.doi.org/10.1016/j.arabjc.2012.12.032
1878-5352 © 2013 Production and hosting by Elsevier B.V. on behalf of King Saud University.
This is an open access article under the CC BY-NC-ND license (http://creativecommons.org/licenses/by-nc-nd/3.0/).

isobutyroyl-hydrazone (H_2AIBuH) have been prepared (Ibrahim, 1992). An octahedral structure was proposed for $[Ni(SIBuH)_2]$, $[Ni(HAIBuH)_2]$, $[Co(SIBuH)–(OAc)(H_2O)]$ and $[Cu(SIBuH)_2]\cdot H_2O$, low-spin octahedral for $[Co(HAIBuH)_2]$ and square-planar for $[Cu(AIBuH)(H_2O)]$. 1,1,3-Propanetetra-salisoyltetracarbo-hydrazone ($H_8PTSTCH$) has multidentate behavior and flexibility to bind in three dimensional space (El-Asmy et al., 1994) to form $[Cu_4(PTSTCH)–(H_2O)_8]\cdot 4H_2O$, $[Co(PTSTCH)(H_2O)_{12}]\cdot\cdot 6H_2O$, $[Sn_4(PTSTCH)–(H_2O)_8]$ and $[(UO_2)_4(PTSTCH)(H_2O)_8]$. Salicyl-aldehyde salicylhydrazone, H_2SS, complexes $[M(HSS)_2]$ (M = Cu^{2+}, Co^{2+}, Mn^{2+}, VO^{2+}, TiO^{2+}), [M'(SS)] (M' = Cu^{2+}, Ni^{2+}, Co^{2+}) and [Cu(HSS)] have been synthesized forming square-planar geometry with Cu^{2+} and octahedral with Ni^{2+} and Co^{2+} (Narang and Aggakwai, 1974). 2-Aceto-1-naphthol-N-salicoylhydrazone was success-fully used for the microdetermination of metal ions in solution (Khattab et al., 1982). Salicaldehyde furonylhydrazone behaves as dibasic ONO forming $[Ni(L)(H_2O)_2]$, $[Co(L)(H_2O)_2]$, [CuL], $[Zn(L)(H_2O)]$, $[Zr(OH)_2(L)–(CH_3OH)_2]$, $[Zr(OH)_2(HL)_2]$, [MoO(L)Cl] and $[UO_2(L)(CH_3OH)]$. The Cu^{2+} and Mo(V)O complexes exhibit subnormal magnetic moments with anti-ferromagnetic interaction (Syamal and Maurya, 1985). Mn^{2+}, Co^{2+}, Ni^{2+}, Cu^{2+} and Zn^{2+} complexes of salicylidene-*N*-cyanoacetohydrazone, H_2L^1 and 2-hydroxy-l-naphthylidene-*N*-cyanoaceto hydrazone, H_2L^2 have been characterized and exhibit octahedral configuration, except $[Co(HL^2)OAc]$ which has tetrahedral structure (Abou El-Enein et al., 2008). No work was done on the ligand under investigation as well as its metal complexes.

2. Experimental

All materials and solvents were used as received. 2,5-Hexanedione, salicaldehyde, and hydrazine hydrate were BDH products. $VOSO_4\cdot H_2O$, $Cr_3(OAc)_7(OH)_2$, $MnCl_2\cdot 4H_2O$, $CoCl_2\cdot 6H_2O$, $Co(OAc)_2\cdot 4H_2O$, $NiCl_2\cdot 6H_2O$, $Ni(OAc)_2\cdot 4H_2O$, $CuCl_2\cdot 2H_2O$ $Cu(OAc)_2\cdot H_2O$ and $Zn(OAc)_2\cdot 2H_2O$ were from Sigma–Aldrich, Germany. Ethanol, methanol, diethylether, acetone, dimethylsulfoxide and dimethylformamide were E. Merk products, and directly used.

2.1. Synthesis of the ligand

The ligand was prepared by similar method reported earlier for 2,5-hexanedione bis(isonicotinyloylhydrazone) (El-Asmy et al., 2010) by the reaction of 0.05 mol of 2,5-hexanedione with 0.1 mol of salicylic acid hydrazide, in 50 ml ethanol. The reaction mixture was boiled under reflux on a water bath for 2 h. After evaporation, the precipitate formed was separated by filtration, recrystallized from ethanol and dried. The preparation procedure is shown as follows:

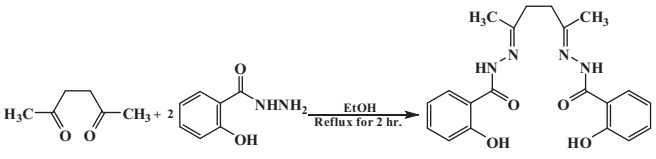

2.2. Synthesis of the complexes

Mononuclear complexes were prepared by heating a mixture of the ligand (3 mmol), dissolved in 20 ml aqueous-ethanol mixed with three drops of 5 M NaOH, and the metal salts (3 mmol) in 30 ml ethanol on a water bath for 1 h. Binuclear complexes were prepared by heating a mixture of the ligand (3 mmol, in NaOH) and the metal salts (6 mmol) in 30 ml aqueous-ethanol solution (v/v) under reflux on a water bath for 4–6 h. The precipitate was filtered off, washed with diethyl ether and finally dried in a vacuum desiccator over anhydrous $CaCl_2$.

2.3. Physical measurements

C, H and N were performed at the Microanalytical Unit of Cairo University. Metal analyses were carried out according to the standard methods (Vogel, 1994). Chloride ion was determined gravimetrically as AgCl. Molar conductance values for the soluble complexes (10^{-3} mol L^{-1}) in DMSO were measured at room temperature (25 ± 1 °C) using a Tacussel conductivity bridge model CD6NG. The IR spectra (KBr disks) were recorded on a Mattson 5000 FTIR Spectrophotometer (400–4000 cm^{-1}). The electronic spectra, as Nujol and/or DMF solution, were recorded on a UV_{2-100} Unicam UV/Vis. The ^1H NMR spectra of H_4L and its Zn^{2+} complex, in d_6-DMSO (300 MHz) were recorded on a Varian Gemini Spectrometer. ESR spectra were obtained on a Bruker EMX spectrometer working in the X-band (9.78 GHz) with 100 kHz modulation frequency. The mass spectrum of the ligand was recorded in Varian MAT 311 Spectrometer. The magnetic moments were measured at 25 ± 1 °C using a Johnson Matthey magnetic susceptibility balance. Thermogravimetric measurements were recorded on a DTG-50 Shimadzu thermogravimetric analyzer. The nitrogen flow and heating rate were 20 ml min^{-1} and 10 °C min^{-1}. The effect of buffer at pH 2–12 on the ligand was carried out by recording the spectra of 0.5 ml of 1×10^{-2} mol l^{-1} of H_4L in EtOH and the measuring flask was completed to 10 ml with aqueous buffer solution having the desired pH without adding supporting electrolyte. The theoretical calculations were performed using Hyper Chem 7.5 program system. The molecular geometry of the ligand was optimized using molecular mechanics (MM+) and then optimized at PM3 using the Polak-Ribiere algorithm.

2.4. Antibacterial activity

The ligand and some complexes were screened against *Sarcina* sp. as Gram positive and *Escherichia Coli* as Gram negative bacteria using the cup-diffusion technique. A 0.2 ml of each (10 μg/ml) was placed in the specified cup made in the nutrient agar medium on which a culture of the tested bacteria has been spread to produce uniform growth. After 24 h incubation at 37 °C, the diameter of inhibition zone was measured as mm.

2.5. Genotoxicity

A solution of 2 mg of Calf thymus DNA was dissolved in 1 ml of sterile distilled water. Stock concentrations of the investigated ligand and its complexes were prepared by dissolving 2 mg/ml DMSO. Equal volumes from each compound and

DNA were mixed thoroughly and kept at room temperature for 2–3 h. The effect of the chemicals on the DNA was analyzed by agarose gel electrophoresis. A 2 µl of loading dye was added to 15 µl of the DNA mixture before being loaded into the well of an agarose gel. The loaded mixtures were fractionated by electrophoresis, visualized by UV and photographed.

2.6. Computational details

The theoretical calculations of the quantum chemistry were performed on a Pentium 4 (3 GHz) computer using Hyper Chem 7.5 program system. The molecular geometry of the ligand was optimized using molecular mechanics (MM+). The low lying obtained from MM+ was then optimized at PM3 using the Polak-Ribiere algorithm in RHF-SCF, set to terminate at an RMS gradient of 0.01 kcal $Å^{-1}$ mol^{-1} and convergence limit was fixed to 1×10^{-8} kcal mol^{-1}.

3. Results and discussion

3.1. Characterization of the ligand

3.1.1. Molecular geometry of H_4L

The atomic numbering scheme and the theoretical geometric structure for H_4L are shown in Scheme 1. Reading the values of the bond lengths and angles, one can observe the formation of intramolecular hydrogen bond [(49)H–O(27)…. H(40)–N(10)] from one side with a bond length of 1.89 ; the other side has no hydrogen bonding. The molecular parameters of the ligand are: total energy (−104472), binding energy (−5309), electronic energy (−785.537), heat of formation (−55.09) kcal/mol; HOMO (−9.1591), LUMO (−0.4474) and the dipole moment (4.024 D).

3.1.2. Effect of solvents and buffer on the ligand

The spectrum of H_4L shows the $\pi \rightarrow \pi^*$ and $n \rightarrow \pi^*$ bands at 38760, 36495, 29940 and 31445 cm^{-1} for the C═O and C═N groups. In water, the main bands are found at 42370, 33555 and 30675 cm^{-1}. The spectrum in benzene (nonpolar molecule) has three bands at 38170, 32465 and 26455 cm^{-1}; the spectrum is changed from polar to nonpolar solvent due to the formation of hydrogen bonding with H_2O. The bands at (43105 and 33110), (41320, 38760, 36765 and 33110 cm^{-1}), and (40000, 32050, 28900 and 26665 cm^{-1}) are observed in CH_3OH, C_2H_5OH, and CH_3Cl, respectively. The spectra are similar in DMF and DMSO with strong bands at 29760 and 29240 cm^{-1}, respectively. In acetone, two weak bands are observed due to the weak solubility.

Examining the spectra at different pHs, the main band due to the nonionic form of the ligand observed at 300 nm is unaltered in the pH range of 2–7. A new band at 326 nm is observed in the pH 10–12 due to the ionic form. The spectrum

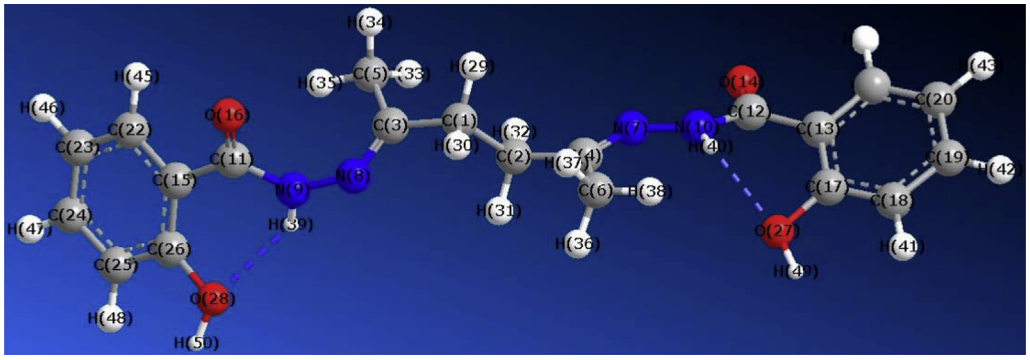

Scheme 1 Molecular modeling of H_4L using HyperChem 7.5 program optimized using molecular mechanics (MM+) at PM3 using the Polak-Ribiere algorithm.

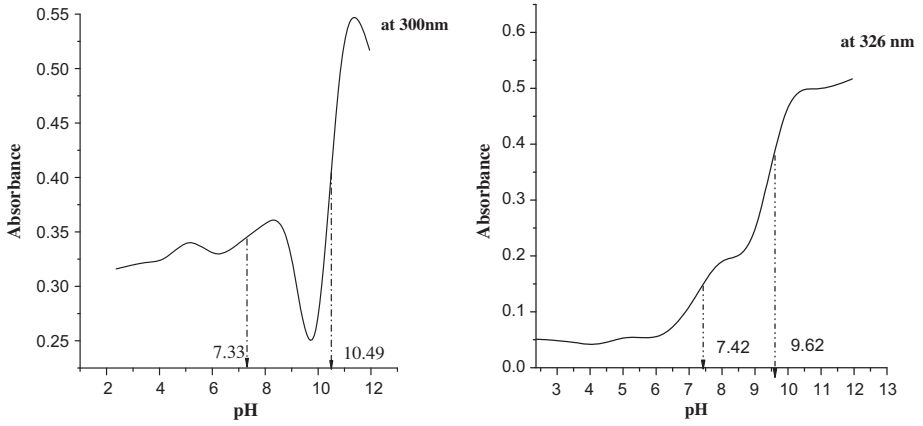

Figure 1 Absorbance-pH relation for the ligand at 300 and 326 nm.

Table 1 Color, melting point and partial elemental analyses of H_4L and its complexes.

Serial no.	Compound	Empirical formula; M.W.	Color	M.P., °C	% Found (Calcd.) C	H	N	Cl	M
1	H_4L	$C_{20}H_{22}N_4O_4$; 382.42	White	175–176	62.6 (62.8)	5.7 (5.6)	14.3 (14.6)		–
2	$[VO(H_2L)]\cdot 2H_2O$	$C_{20}H_{24}N_4O_7V$; 483.40	Brown	> 300	49.7 (49.7)	5.0 (5.0)	11.311.5)		
3	$[Cr_2(H_2L)(OAc)_2(OH)_2]\cdot 2H_2O$	$C_{24}H_{32}N_4O_{12}Cr_2$; 671.92	Paige	> 300	42.4 (42.8)	5.1 (4.8)	8.1 (8.3)		15.3 (15.5)
4	$[Mn_2(H_2L)(OH)_2]\cdot H_2O$	$C_{20}H_{24}N_4O_7Mn_2$; 542.24	Paige	> 300	44.5 (44.3)	4.4 (4.5)	9.9 (10.3)	–	19.9 (20.2)
5	$[Co_2(H_2L)(H_2O)_4Cl_2]\cdot 2H_2O$	$C_{20}H_{32}N_4O_{10}Cl_2Co_2$;676.80	Brown	> 300	35.3 (35.5)	3.7 (4.7)	7.7 (8.3)	9.9 (10.5)	16.9 (17.4)
6	$[Co_2(H_2L)(OAc)_2]\cdot H_2O$	$C_{24}H_{28}N_4O_9Co_2$; 636.41	Brown	> 300	45.8 (45.3)	4.2 (4.4)	9.1 (8.8)		19.0 (18.5)
7	$[Ni(H_4L)Cl_2]\cdot 2H_2O$	$C_{20}H_{26}N_4O_6Cl_2Ni$; 548.11	Brown	> 300	44.2 (43.8)	5.2 (4.8)	9.9 (10.2)	13.5 (13.0)	10.2 (10.7)
8	$[Ni(H_2L)]\cdot 3H_2O$	$C_{20}H_{26}N_4O_7Ni$; 493.14	Yellow	275–276	50.0 (49.0)	5.1 (5.3)	10.9 (11.4)		11.8 (11.9)
9	$[Cu(H_4L)(H_2L)(EtOH)_2]\cdot 2H_2O$	$C_{44}H_{58}N_8O_{12}Cu$; 897.50	Brown	> 300	58.3 (58.8)	5.9 (6.5)	12.0 (12.5)	–	6.9 (7.1)
10	$[Cu_2(H_2L)(OAc)_2(H_2O)_6]$	$C_{24}H_{38}N_4O_{14}Cu$; 733.5	Brown	> 300	38.9 (39.3)	4.8 (5.5)	8.6 (8.9)		17.5 (17.3)
11	$[Zn(H_2L)]$	$C_{20}H_{20}N_4O_4Zn$; 445.75	White	> 300	53.6 (53.9)	4.5 (4.5)	12.2 (12.6)		14.6 (14.7)

Table 2 IR spectral data of H_4L and its metal complexes.

Serial No.	ν(OH)	δ(OH)	ν(NH)	ν(C=N)	ν(C=N[a])	ν(C=O)	ν(CO)	υ(M–O)	υ(M–N)
1	3290	1368	3039	1626	–	1644	–	–	–
2	–	–	3099	1610	–	1652	–	526	464
3	3389[a]	1399		1605	–	1605	1247	532	437
	3278	1326[a]							
4	3446[b]	1373		1612	1577	–	1249	539	424
	3426	1328[a]							
	3384[a]								
5	3590	1374	–	1594	1532	–	1253	529	423
	3440[b]								
6	3410	1378	–	1603	1565	–	1248	533	464
7	3370(br)	1363	3279	1609	–	1633	1242	530	431
8	3316	1375	–	1600	1536	–	1258	498	440
9	3412(br)	1375	3078	1607	1531	1653	1223	531	486
10	3411	1378	–	1599	1534	–	1252	491	463
11	3199	1376	–	1598	1542	–	1257	499	427

[a] the OH vibration of hydroxo group;
[b] the hydrated H_2O.

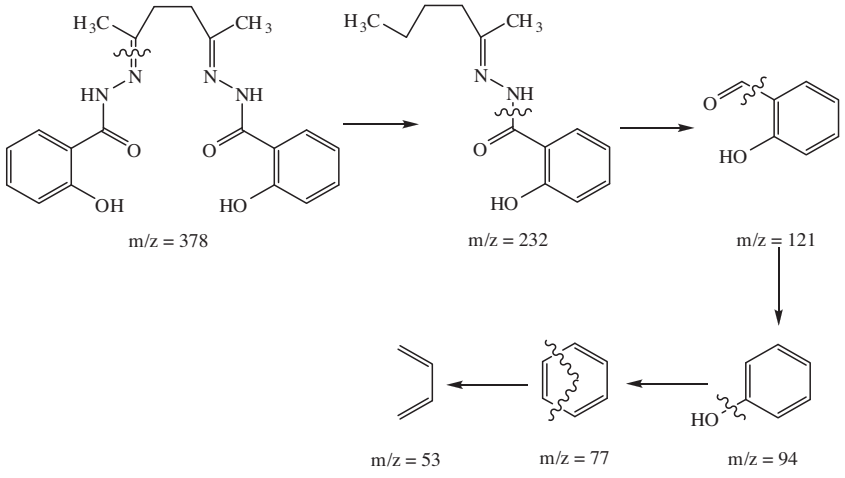

Scheme 2 Fragmentation pattern of the ligand.

Table 3 Magnetic moments and electronic spectral bands of the compounds.

Serial No.	μ_{eff} (BM)[a]	State	Intraligand and charge-transfer (cm^{-1})	d–d transition (cm^{-1})	Ligand field parameters B; β; Dq	Suggested geometry
1	–	DMSO	36495; 33780; 31445; 29940	–	–	
2	0.71	DMF	35710; 32255; 27930; 23040			Square-based pyramid
		Nujol	24390, 23580, 21920, 20745	19530; 19375; 17360		
3	3.92	DMSO	33110; 27470	20325; 16775	335.3; 0.365; 1677	Octahedral
		Nujol	25510, 24035, 22830	21095; 17855	457.9; 0.498; 1786	
4	6.38	Nujol	25380, 24630, 23580, 21830	19157; 17120		Tetrahedral
5	4.53	DMF	35710; 33330; 28405; 25905	20660		
		Nujol	25510, 24750, 22830	20745;18725; 17605	889.6; 0.916; 979	Octahedral
6	4.27	DMF	35710; 33330; 27930; 25125	22620	483.5; 0.498; 689	Tetrahedral
		Nujol	24270, 22725, 22025	20490; 19530; 17540		
7	3.21	DMF	36495; 33330; 31445; 29760; 28405	21185		Octahedral
		DMSO	36495; 33555; 31250;29760; 28245	21095		
		Nujol	23255, 21455, 20575	19840; 18515; 17240; 14880	454.0; 0.44;1044	
8	3.47	DMF	35710; 32675; 29940;	23145; 21925		Tetrahedral
		DMSO	35460; 32050; 28405	23920; 22935; 21645; 17920; 15475		
		Nujol	25250, 22935, 21645	20325,19155; 17120		
9	1.77	DMF	35970; 33330; 27775; 25905	————	Octahedral	
		Nujol	24630, 23145, 21459	19455;18655; 17120		
10	2.09	DMF	35710; 33330; 27920; 23470	16285		Octahedral
		DMSO	24035; 21735	20080; 18180		
		Nujol	25510, 23470, 21645			
11	–	DMSO	37035; 35460; 25250;	31645; 29940	-	Tetrahedral

[a] The value calculated for one metal ion.

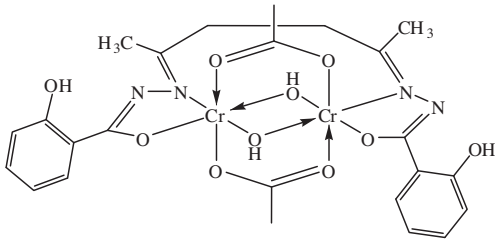

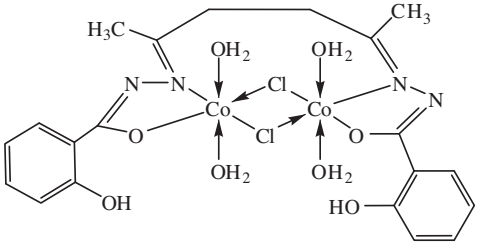

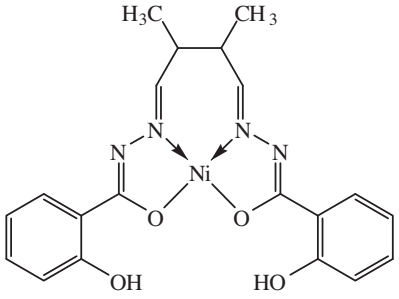

Scheme 3 Structures of $[Cr_2(H_2L)(OAc)_2(OH)_2]\cdot 2H_2O$, $[Co_2(H_2L_1)(H_2O)_4Cl_2]\cdot 2H_2O$ and $[Ni((H_2L)]\cdot 3H_2O$.

at pH 7–9 has two bands at 300 and 326 nm representing the pH at which the two forms exist in equilibrium. The values [7.42 (7.33), 9.62 (10.49)] are nearly similar at the two wavelengths 326 (300 nm). The first may be due to the liberation of the amidic proton (CONH) while the second is due to the phenoxy proton (OH). The relation between the absorbance and pH at two wavelengths (Fig. 1) was used to calculate the pK's of the ligand. The curves are characterized by two well defined s-shapes denoting the presence of two pK's. The pK in each s-shape is calculated by the half height method (Issa et al., 1973).

3.1.3. IR, ^1H NMR and MS spectra of the ligand

The IR assignments of H_4L bands are included in Table 2. The spectrum shows bands at 3290, 3090, 1644, 1626 and 1368 cm^{-1} assigned to υ(OH), υ(NH), υ(C═O), υ(C═N) and δ(OH) vibrations, respectively. The ^1H NMR spectrum shows signals at 12.44 and 11.19 ppm for the OH protons (due to the presence of the two −OH in different planes) one in the plane while the other is out-of-plane. The signal at 10.02 ppm is due to the NH proton while the multiple signals at 7.88–6.82 ppm are due to the phenyl groups. The CH_3 and CH_2 protons appeared at 2.04 and 3.32 ppm. On deuteration, the signals of OH and NH disappeared. The mass spectrum of H_4L reveals the molecular ion peak $[M-4]^+$ at $m/z = 378$ (Mol. Wt. = 382). The fragmentation pattern of the ligand is represented in Scheme 2.

3.2. Characterization of the complexes

VO^{2+}, Cr^{3+}, Mn^{2+}, Co^{2+}, Ni^{2+}, Cu^{2+} and Zn^{2+} ions have the ability to form complexes with H_4L having the formulae: $[VO(H_2L)]\cdot 2H_2O$, $[Ni(H_2L)]\cdot 3H_2O$, $[Zn(H_2L)]$, $[Ni(H_4L)Cl_2]\cdot 2H_2O$, $[Cu(H_4L)(H_2L)\text{-}(EtOH)_2]\cdot 2H_2O$, $[Co_2(H_2L)\text{-}(OAc)_2]\cdot$

H_2O, $[Cr_2(H_2L)(OAc)_2(OH)_2]\cdot 2H_2O$, $[Cu_2(H_2L)(OAc)_2(H_2O)_6]$, $[Mn_2(H_2L)(OH)_2]\cdot H_2O$ and $[Co_2(H_2L)(H_2O)_4Cl_2]\cdot 2H_2O$ (Table 1). The source of OH in the Cr^{3+} complex is the metal salt and in the Mn(II) complex from the reaction in basic medium. The complexes are insoluble in most common organic solvents but are completely soluble in DMSO. The molar conductance values, for 10^{-3} mol L^{-1} solution, were in agreement with non-electrolytes (Bahgat and Orabi, 2002).

3.2.1. IR and ^1H NMR spectra of the complexes

Examining the IR spectra of the complexes (Table 2) one may conclude the following:

(i) In all complexes, the υ(C═N) in the ligand is shifted to lower wavenumber with the appearance of a new band due to υ(M–N) indicating the participation of this group in bonding.
(ii) In most complexes, the υ(OH) appeared as medium or broad band at higher wavenumbers proving the destruction of the hydrogen bond accompanied by new bands attributed to the hydroxo bridge (OH) in $[Cr_2(H_2L)(OAc)_2(OH)_2]\cdot 2H_2O$ and $[Mn_2(H_2L)(OH)_2]\cdot H_2O$ (Kumar et al., 2009) as well as the hydrate H_2O. This observation is supported by the appearance of δ(OH) more or less at the same position with another band at 1328 cm^{-1} due to the δ(OH) of hydroxo group.
(iii) In [VO(H2L)]·2H2O, the υ(OH) and δ(OH) bands disappear revealing the deprotonation of the phenolic OH and its participation in bonding.
(iv) In most complexes, the (C═O) and (NH) bands disappear indicating the enolization of CONH and the CO group is participating in coordination. Evidence is the appearance of new bands at 1531–1577 and 1223–1258 cm^{-1} due to υ(C═N*) and υ(CO) vibrations. In $[VO(H_2L)]\cdot 2H_2O$ and $[Ni(H_4L)Cl_2]\cdot 2H_2O$, the C═O and NH bands still existing at the same position.
(v) In $[Cu(H_3L)_2(EtOH)_2]\cdot 2H_2O$, the (C═O) and (NH) bands appear very weak at the same position indicating that the ligands coordinate in the keto-enol form. In $[Cr_2(H_2L)(OAc)_2(OH)_2]\cdot 2H_2O$, $[Co_2(H_2L)(OAc)_2]\cdot H_2O$ and $[Cu_2(H_2L)(OAc)_2(H_2O)_6]$, the acetate groups act as bridged bidentate confirming by the appearance of two bands in the regions 1599–1605 and 1435–1447 cm^{-1} with difference ≈150 cm^{-1} (Adams et al., 2002).
(vi) The appearance of bands due to υ(M–O), υ(M–OH) and υ(M–OH_2) at ≈528 and ≈3347 due to the hydrated water. The bands at 3292, 930 and 600 cm^{-1} in $[Cu_2(H_2L)(OAc)_2(H_2O)_6]$ and $[Co_2(H_2L)(H_2O)_4Cl_2]\cdot 2H_2O$ are attributed to υ(OH), $\rho_r(H_2O)$ and $\rho_w(H_2O)$ of coordinated water (El-Asmy and Al-Hazmi, 2009).
(vii) The ^1H NMR spectrum of $[Zn(H_2L)_2]$ shows a signal at 13.65 ppm attributed to the OH proton with the disappearance of the NH proton. On deuteration, the OH signal disappeared.

3.2.2. Spectral and magnetic studies

The magnetic moments and the significant electronic absorption bands of the complexes, recorded in DMF or Nujol mull, are given in Table 3 (DMF has no effect on the color).

The spectrum of H_4L shows the $\pi \rightarrow \pi^*$ and $n \rightarrow \pi^*$ bands at 36495, 38780, 31445 and 29940 cm^{-1} for the C═O and C═N groups. A change is observed on the spectra of its complexes. The bands at 25250–28405 and 23040–25905 cm^{-1} in the spectra of the complexes may be due to LMCT from N and O donors.

The two bands at 23040 and 19530 cm^{-1} in the spectrum of $[VO(H_2L)]\cdot 2H_2O$ in DMF is assigned to the $d_{xz} \rightarrow d_{xy}$ transition (El-Metwally et al., 2005) in a square-pyramidal geometry. In Nujol, multiple bands are appeared at 17360, 19375, 20745, 21920, and 23580 cm^{-1} with additional broad band centered at 24390 cm^{-1} due to a charge-transfer. Its magnetic moment (0.71 BM) is anomalous for one unpaired electron which may be due to interaction with neighboring molecules.

The spectrum of $[Cr_2(H_2L)(OAc)_2(OH)_2]\cdot 2H_2O$, in DMSO, shows bands at 16775 and 20325 cm^{-1} attributed to $^4A_{2g}$ (F) → $^4T_{2g}$ (P) (ν_1) and $^4A_{2g}$ (F) → $^4T_{1g}$ (F) (ν_2), in an octahedral geometry (Aranha et al., 2007) (Scheme 3). In Nujol, these bands are observed at 17855, 21095 and 22830 cm^{-1}. In addition, a band at 24035 cm^{-1} is due to a charge-transfer. The ligand field parameters, in DMSO (Nujol) [Dq = 1676.7 (1785.8) cm^{-1}, B = 335.3 (457.9) cm^{-1} and β = 0.365 (0.498)] further supported the proposed geometry. The lower value of β indicates more covalency. Its magnetic moment (3.92 BM) is normal for three unpaired electrons with no orbital contribution.

The electronic spectrum of $[Co_2(H_2L)(H_2O)_4Cl_2]\cdot 2H_2O$, in Nujol, shows bands at 18725 and 20745 cm^{-1} assigned to $^4T_{1g} \rightarrow {}^4A_{2g}$ (ν_2) and $^4T_{1g} \rightarrow {}^4T_{1g}$ (P) (ν_3) characteristic for an octahedral geometry (Chandra et al., 2006). In DMF solution, only band is observed at 20660 cm^{-1}. The band due to $^4T_{1g} \rightarrow {}^4T_{1g}$ (ν_1) is not observed and calculated to be 9785 cm^{-1}. The B, β and $10Dq$ values (Table 3) agree with those reported for octahedral Co^{2+} complexes. The value of β indicates a strong covalent bond. The μ_{eff} value for each metal ion is 4.53 BM is slightly lower than the values reported for complexes having the proposed geometry (Scheme 3) may be due to interaction between the two metal atoms.

The spectra of $[Co_2(H_2L)(OAc)_2]\cdot H_2O$ in Nujol (DMF) show bands at 22025 (22620) cm^{-1} attributed to $^4A_2 \rightarrow {}^4T_1$ (ν_3) similar to those reported for tetrahedral complexes (Efthimiadou et al., 2007]. The B, β and $10Dq$ values (Table 3) agree with those reported for tetrahedral Co^{2+} complexes. Reduction in the B and β values indicates a covalent character of L–M bonds. The value of β indicates a strong covalent bond. The ν_1 ($^4A_2 \rightarrow {}^4T_2$) is calculated to be 6889 cm^{-1}. The complex shows additional bands at 17540 and 19530 cm^{-1} in a tetrahedral structure (El-Shazly et al., 2006) around the Co^{2+} ion.

The magnetic moment (3.21 BM) of $[Ni((H_4L)Cl_2]\cdot 2H_2O$ is expected for octahedral structure with $^3A_{2g}$ ground term (Singh and Singh, 2001). Its electronic spectrum shows broad bands in Nujol at 23255 (ν_3) and 14880 cm^{-1} (ν_2) assigned to $^3A_{2g} \rightarrow {}^3T_{1g}$ (F) (ν_2) (Lal et al., 2009). The values of B (454 cm^{-1}) and $10Dq$ (10442 cm^{-1}) are used to calculate β and ν_1, $^3A_{2g} \rightarrow {}^3T_{2g}$ (F), to be 0.44 and 10442 cm^{-1}, respectively (Abd El-Wahab, 2007). The spectra in DMF and DMSO are similar showing only band at ≈21100 cm^{-1}.

The magnetic moment (3.47 BM) of $[Ni((H_2L)]\cdot 3H_2O$ lies within the range reported for a tetrahedral structure. Its electronic spectrum in Nujol shows bands at 20325, 19155 and 17120 cm^{-1} falling in the range reported for the proposed geometry (Scheme 3) (El-Shazly et al., 2005).

The electronic spectrum of $[Cu(H_3L)_2(EtOH)_2]\cdot 2H_2O$ exhibits bands at 17120 19155, 22220 cm^{-1} in Nujol assigned

Table 4 Decomposition steps for the complexes.

Complex	Temp. range, °C	Removed species	Weight loss % Found (Calcd)
$[VO(H_2L)]\cdot 2H_2O$	38–129	$-2H_2O$	5.8(5.7)
	130–341	$-(C_6H_{10} + 2OH)$	24.7(24.5)
	342–547	$-(C_{14}H_8O_2)$	44.4(43.9)
	549–718	$-2N_2$	11.4(11.8)
	719–800	VO (Residue)	13.7(13.9)
$[Ni(H_2L)]\cdot 3H_2O$	70–134	$-3H_2O$	11.7(11.0)
	253–344	$-(C_7H_6NO + C_2H_4 + CH_3)$	32.8(33.1)
	346–653	$-(C_7H_6NO + CH_3)$	27.5(27.3)
	654–793	$-(2(C = N) + 0.5O_2)$	11.3(13.78)
	794–800	NiO (Residue)	15.46(14.6)
$[Co_2(H_2L)(OAc)_2]\cdot H_2O$	50–125	$-H_2O$	2.8(2.8)
	239–334	$-C_6H_{10+}2OH$	18.6(18.2)
	334–475	$-(C_{14}H_8 + 2N_2 + 2AcO)$	55.1(55.0)
	476–800	2CoO (Residue)	23.5(23.3)
$[Zn(H_2L)]$	168–360	$-2C_7H_6N$	46.8(46.4)
	361–481	$-C_4H_{10}$	12.8(12.9)
	482–555	$-2C = N + 1.5O_2$	(22.3)(18.2)
	556–800	ZnO (Residue)	
$[Mn_2(H_2L)(OH)_2]\cdot H_2O$	29–82	$-H_2O$	2.9(3.4)
	287–410	$-(2C_6H_5O + C_6H_{10} + 2N_2 + C_2)$	64.9(64.2)
	411–800	2MnO (Residue)	25.3(26.1)
$[Cu_2(H_2L)(OAc)_2(H_2O)_6]$	203–399	$-(2C_7H_6NO + C_2H_4 + CH_3 + 6H_2O)$	53.0(53.3)
	399–545	$-(CH_3 + C = N + AcO)$	14.4(13.6)
	546–773	$-(C = N + AcO)$	12.7(11.6)
	773–800	2CuO (Residue)	19.9(21.5)
$[Cr_2(H_2L)(OAc)_2(OH)_2]\cdot 2H_2O$	36–137	$-2H_2O$	6.0(5.4)
	225–327	$-(C_6H_{10} + 2OH)$	17.4(17.3)
	327–431	$-(C_{14}H_{10}N_4O + 2AcO + OH)$	55.0(54.7)
	431–800	Cr_2O_3 (Residue)	21.6(22.6)

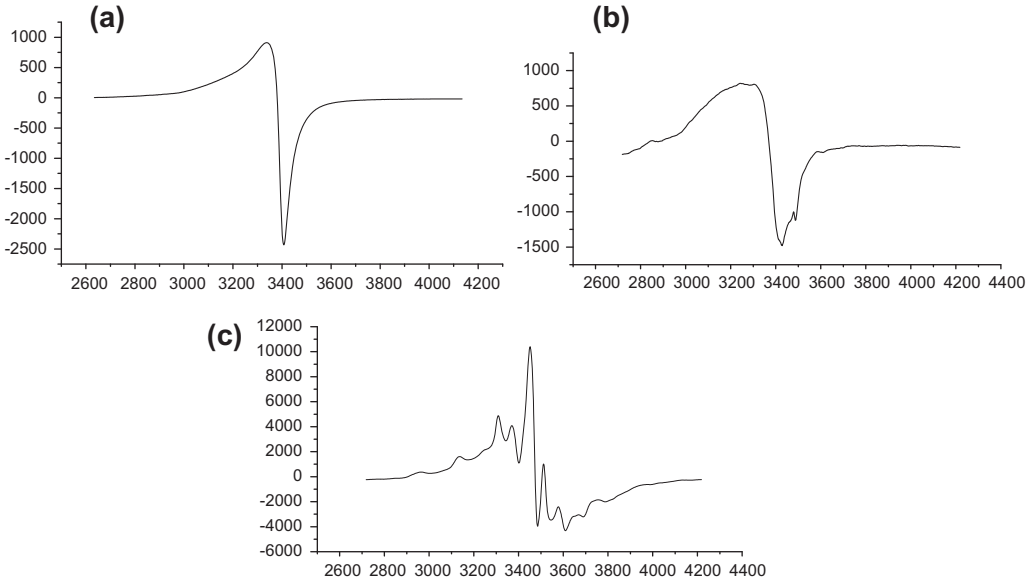

Figure 2 The ESR spectra of (a) $[Cu_2(H_2L)(OAc)_2(H_2O)_6]$; (b) $[Cu(H_4L)(H_2L)(EtOH)_2]\cdot 2H_2O$ and (c) $[VO(H_2L)]\cdot 2H_2O$.

to $^2T_{2g} \rightarrow {}^2E_g$ and a symmetric forbidden ligand–metal charge-transfer. In DMF, no observed bands for the d–d transitions but the band appearing at 25905 cm^{-1} is mainly due to a charge-transfer. The band positions with magnetic moment of 1.77 BM are consistent with an octahedral geometry (Manoj et al., 2009). The spectrum of $[Cu_2(H_2L)(OAc)_2(H_2O)_6]$ in Nujol exhibits bands at 18180 and 20080 cm^{-1} assigned to $^2T_{2g} \rightarrow {}^2E_g$ and a symmetric forbidden ligand–metal charge-transfer. In DMSO, these bands are observed at 16285 and 21735. The broadness of the first band may be due to

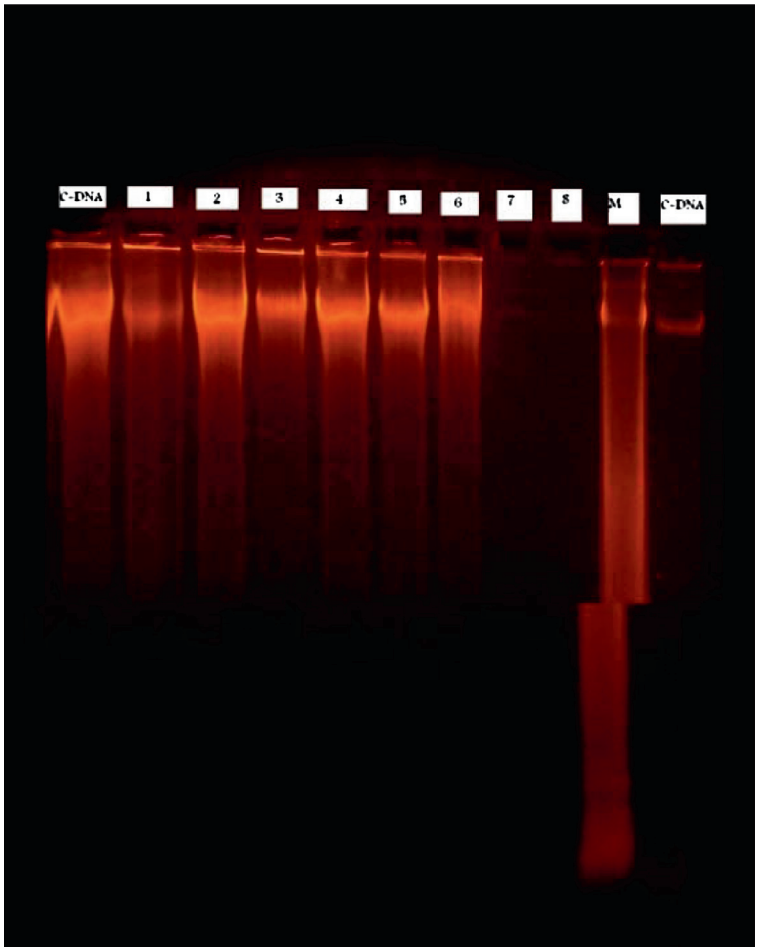

Figure 3 Biological effect of H_4L and its complexes on the Calf Thymus DNA Lanes arranged as: C-control DNA, 1-Ligand, 2-$[VO(H_2L)]\cdot 2H_2O$, 3-$[Cr_2(H_2L)(OAc)_2(OH)_2]\cdot 2H_2O$, 4-$[Mn_2(H_2L)(OH)_2]\cdot H_2O$, 5-$[Co_2(H_2L)(H_2O)_4Cl_2]\cdot 2H_2O$, 6-$[Co_2(H_2L)(OAc)_2]\cdot H_2O$, 7-$[Ni(H_4L)Cl_2]\cdot 2H_2O$ and 8-$[Zn(H_2L)]$.

Table 5 Parameters of the molecular modeling of H_4L_1 complexes.

Parameters	Total energy (kcal/mol)	Binding energy (kcal/mol)	Heat of formation (kcal/mol)	Electronic energy (kcal/mol)	Nuclear energy (kcal/mol)	Dipole moment (Debyes)	HOMO (eV)	LUMO (eV)
2	−159729	−5029	413	−1376200	1216471	7.562	−8.83343	−2.76606
3	−128285	−4028	437	−954834	826549	0	−9.10911	−2.32027
4	−171110	−5162	176	−1340384	1169273	1.873	−9.39293	−2.12368
8	−117365	−4122	652	−839924	722558	1.560	−9.09869	−2.19626
7	−135331	−3863	509	−967888	832556	6.428	−8.31821	−2.75733
11	−96501	−3339	799	634367	537865	0	−9.04210	−2.54182

Jahn–Teller effect which enhances the distortion in octahedral geometry (Al-Hazmi et al., 2005). The magnetic moment (2.09 BM) for each copper atom is consistent with one unpaired electron in an octahedral geometry.

The electronic spectrum of $[Mn_2(H_2L)(OH)_2]\cdot H_2O$ exhibits multiple weak bands at 17120, 21830 23580 and 24630 cm^{-1} assignable to the transitions in a tetrahedral structure. The magnetic moment (6.38 BM) is corresponding to five unpaired electrons with orbital contribution in a high spin geometry (PUI, 2007).

3.2.3. Thermal studies

The thermogravimetric data considering the decomposition temperature range, the removed species and the weight losses for most complexes are presented in Table 4. Example for one mononuclear complex and binuclear complex is described here in detail.

The steady part of the thermogram of $[Zn(H_2L)]$ (Scheme 4) till 167 °C indicates the absence of any solvent outside the sphere. The 1st decomposition step starting at 168–360 °C is due to the removal of two phenolic rings $\{2C_6H_5O\}$ (% Found

41.9; Calcd. 41.7). The 2nd step (361–481 °C) indicates the decomposition of $\{C_6H_{10}\}$ (% Found 18.7; Calcd. 18.4). The last step (482–555 °C) shows the decomposition of $\{2N_2 + CO + C\}$ (% Found 21.8; Calcd. 21.5). ZnO is the stable residue at 800 °C (% Found 18.0; Calcd. 18.3).

In $[Cr_2(H_2L)(OAc)_2(OH)_2]\cdot 2H_2O$, the TG curve is characterized by steps at 36–137, 138–327, 328–431 and 432–800 °C corresponding to the removal of outside water (% Found 6.0; Calcd. 5.4), C_6H_{10} + 2OH (% Found 17.4; Calcd. 17.3) and $C_{14}H_{10}N_4O$ + 2OAc + OH (% Found 55.0 Calcd. 54.7) after which the residue is Cr_2O_3 (% Found 21.6; Calcd. 22.6).

3.2.4. ESR spectra

To obtain further information about the stereochemistry of VO^{2+} and Cu^{2+} complexes, ESR spectra were recorded and their spin Hamiltonian parameters were calculated.

The room temperature solid state ESR spectra of the copper complexes [Fig. 2(a and b)] exhibit an axially symmetric g-tensor parameters with $g_{||} > g_{\perp} > 2.0023$ indicating that the copper site has a $d_x^2 - d_y^2$ ground state (Kasumov et al., 2004). In axial symmetry, the g-values are related by the expression, $G = (g-2)/(g_{\perp}-2) = 4$. According to Hathaway (Hathaway and Billing, 1970; Hathaway, 1984), as value of G is greater than 4, the exchange interaction between Cu^{2+} centers in the solid state is negligible, whereas when it is less than 4, a considerable exchange interaction is indicated in the solid complex. The calculated G values for the copper complexes are less than 4 suggesting copper–copper exchange interactions. The ESR spectrum of $[Cu_2(H_2L)(OAc)_2(H_2O)_6]$ is similar to the ESR spectra of the reported binuclear Cu^{2+} complexes (Khan et al., 1989). The ESR spectrum of $[Cu(H_3L)_2(EtOH)_2]\cdot 2H_2O$ exhibits a single line centered at $g_{//} = 2.25$ and $g// = 2.07$, respectively, (Fig. 1b) attributable to dipolar broadening and enhanced spin lattice relaxation. This line is probably due to insufficient spin-exchange narrowing toward the coalescence of four copper hyperfine lines to a single line. Note that, the same kind of powder ESR line shapes has been observed for many tetrahedral or square-planar binuclear Cu^{2+} complexes with a strong intranuclear spin-exchange interaction.

Molecular orbital coefficients, α^2 and β^2 were calculated (John et al., 2003):

$$\alpha^2 = (A_{//}/0.036) + (g_{//} - 2.0023) + 3/7(g_{\perp} - 2.0023) + 0.04 \quad (1)$$

$$\beta^2 = (g_{//} - 2.0023)E/ - 8\lambda\alpha^2 \quad (2)$$

where $\lambda = -828\ cm^{-1}$ for Cu^{2+} and E is the electronic transition energy. $\alpha^2 = 1$ indicates complete ionic character, whereas $= 0.5$ denotes 100% covalent bonding with negligibly small values of the overlap integral. The β^2 parameter gives an indication of the covalency of the in-plane π-bonding. The smaller the β^2 the larger is the covalency of the bonding.

The values of α^2 and β^2 for the complexes indicate that the in-plane σ-bonding and in-plane π-bonding are appreciably covalent, and are consistent with very strong in-plane σ-bonding in these complexes. For the Cu^{2+} complexes, the high values of β^2 compared to α^2 indicate that the in-plane π-bonding is less covalent than the in-plane σ-bonding. These data are well consistent with other reported values.

The ESR spectrum of $[VO(H_2L)]\cdot 2H_2O$ (Fig. 1c) provides a characteristic octet ESR spectrum showing the hyperfine coupling to the ^{51}V nuclear magnetic moment and similar to those reported for mononuclear vanadium molecule (Thaker et al., 1994). In the powdered form for the mono vanadium complex, the spectrum showed the parallel and the perpendicular features which indicate axially symmetric anisotropy with well resolved sixteen-lines hyperfine splitting characteristic for the interaction between the electron and the vanadium nuclear spin ($I = 7/2$) (Khasa et al., 2003). The spin Hamiltonian parameters are calculated to be $g_{//}(1.93)$, $g_{\perp}(1.96)$, $A_{//}(200 \times 10^{-4}\ cm^{-1})$ and $A_{\perp}(60)$. The calculated ESR parameters indicate that the unpaired electron (d^1) is present in the d_{xy}-orbital with square-pyramidal or octahedral geometry (Raman et al., 2003). The values obtained agree well with the g-tensor parameters reported for square pyramidal geometry.

The molecular orbital coefficients α^2 and β^2 for complex (2) are calculated using the reported equations (Warad et al., 2000) and found to be 0.92 and 0.83, respectively. The low value of β^2 than α^2 indicates that the in-plane σ-bonding is less covalent and consistent with other reported data (Georgieva et al., 2006).

3.2.5. Antimicrobial activity

The ligand and its metal complexes were tested against Gram-positive, Bacillus thuringiensis (BT), H_4L is more effective on BT than the complexes.

3.2.6. Eukaryotic DNA degradation test

Examining the DNA degradation assay of H_4L and its metal complexes, one can conclude variability on their immediate damage on the calf thymus (CT) DNA. The complexes have higher effect on the calf thymus DNA than the ligand. $[VO(H_2L)]\cdot 2H_2O$, $[Cr_2(H_2L)(OAc)_2(OH)_2]\cdot 2H_2O$, $[Mn_2(H_2L)(OH)_2]\cdot H_2O$, $[Co_2(H_2L)(H_2O)_4Cl_2]\cdot 2H_2O$, and $[Co_2(H_2L)(OAc)_2]\cdot H_2O$ have little effect while the $[Ni(H_4L)Cl_2]\cdot 2H_2O$ and $[Zn(H_2L)]$ complexes degrading the CT DNA completely (Fig. 3). $[Cr_2(H_2L)(OAc)_2(OH)_2]\cdot 2H_2O$ and the ligand have similar effect. The results suggest that direct contact of $[Ni(H_4L)Cl_2]\cdot 2H_2O$ and $[Zn(H_2L)]$ is necessary to degrade the DNA of Eukaryotic subject.

3.2.7. Molecular modeling of the complexes

The molecular modeling of the complexes is presented. The molecular parameters of the complexes are shown in Table 5. Inspection of the data, it is observed that:

(i) All complexes have dipole moment values except $[Mn_2(H_2L)(OH)_2]\cdot H_2O$ and $[Zn(H_2L)]$ which have zero moment; this may be due to the trans-form of the complexes; the highest one is $[Cr_2(H_2L)(OAc)_2(OH)_2]\cdot 2H_2O$ which is considered as a strong polar molecule.
(ii) Comparing the data of the two Ni(II) complexes, one can observe that $[Ni(H_2L)]\cdot 3H_2O$ has a lower moment than $[Ni(H_4L)Cl_2]\cdot 2H_2O$ suggesting that the oxygen and nitrogen atoms exist in opposite side (Scheme 8).
(iii) The shape of $[Zn(H_2L)]$ (Scheme 10) is found tetrahedral rather than a square-planar and this expected for the d^{10}-system with sp^3 hybridization.

(iv) All heats of formation are positive and arranged the complexes as: $[Zn(H_2L)] > [Ni(H_2L)]\cdot 3H_2O > [Ni(H_4L)Cl_2]\cdot 2H_2O > [Mn_2(H_2L)\text{-}(OH)_2]\cdot H_2O > [Cr_2(H_2L)(OAc)_2(OH)_2]\cdot 2H_2O > [Co_2(H_2L)(OAc)_2]\cdot H_2O$.

The bond lengths and angles of the compounds are listed in Supplementary Tables 1S–7S.

4. Conclusion

2,5-Hexanedione bis(salicyloylhydrazone) has been prepared and characterized. Its molecular geometry is predicted by molecular modeling using MM+ and PM3 methods and its bond lengths and angles are calculated. It showed multidentate behavior with four ionizable protons. Its ionization constants are 7.42 and 9.62 representing the amide and hydroxo protons. Its UV spectrum is changed from polar to nonpolar solvents. The IR spectra give evidence for coordination of the ligand through the NO donor atoms and the NMR spectra supported the coordination sites. The magnetic measurement and the electronic spectra suggested that the formed complexes having tetrahedral: $[Co_2(H_2L)(OAc)_2]\cdot H_2O$, $[Ni(H_2L)]\cdot 3H_2O$ and $[Zn(H_2L)]$; square-pyramidal: $[VO(H_2L)]\cdot 2H_2O$ and octahedral for the rest. The stable oxides VO, Cr_2O_3, CoO, NiO, ZnO and MnO remain as residues at the end step of TGA. The DNA degradation assay for the compounds suggests that direct contact of $[Ni(H_4L)Cl_2]\cdot 2H_2O$ and $[Zn(H_2L)]$ is necessary to degrade the DNA of Eukaryotic subject.

Appendix A. Supplementary data

Supplementary data associated with this article can be found, in the online version, at http://dx.doi.org/10.1016/j.arabjc.2012.12.032.

References

Abd El-Wahab, Z.H., 2007. Spectrochim. Acta 67A, 25.

Abou El-Enein, S., El-Saied, F.A., Emam, S.M., El-Salamony, M.A., 2008. Spectrochim. Acta 71A, 421.

Adams, H., Clunas, S., Fenton, D.E., 2002. Inorg. Chem. Commun. 15, 1063.

Al-Hazmi, G.A.A., El-Shahawi, M.S., Gabr, I.M., El-Asmy, A.A., 2005. J. Coord. Chem. 58 (8), 713.

Aranha, P.E., dos Santos, M.P., Romera, S., Dockal, E.R., 2007. Polyhedron 26, 1373.

Bahgat, K.H., Orabi, A.S., 2002. Polyhedron 21, 987.

Chandra, S., Kumar, R., Singh, R., Jain, A.Kr., 2006. Spectrochim. Acta 65A, 852.

Efthimiadou, E.K., Sanakis, Y., Katsaros, N., Karaliota, A., Psomas, G., 2007. Polyhedron 26, 1148.

El-Asmy, A.A., Al-Abdeen, A.Z., Abo El-Maaty, W.M., Mostafa, M.M., 2010. J. Spectrochim. Acta 75A, 1516.

El-Asmy, A.A., Al-Ansi, T.Y., Mabrouk, H.E., Amin, R.R., 1994. Qatar Univ. Sci. J. 14, 88.

El-Asmy, A.A., Al-Hazmi, G.A.A., 2009. Spectrochim. Acta 71A, 1885.

El-Metwally, N.M., El-Shazly, R.M., Gabr, I.M., El-Asmy, A.A., 2005. Spectrochim. Acta 61A, 1113.

El-Shazly, R.M., Al-Hazmi, G.A.A., Ghazy, S.E., El-Shahawi, M.S., EI-Asmy, A.A., 2006. J. Coord. Chem. 59 (8), 846.

El-Shazly, R.M., El-Hazmi, G.A., Ghazy, S.E., El-Shahawi, M.S., El-Asmy, A.A., 2005. Spectrochim. Acta 61A, 243.

Georgieva, I., Trendafilova, N., Bauer, G., 2006. Spectrochim. Acta 63, 403.

Hathaway, B.J., 1984. Struct. Bonding (Berlin) 57, 55.

Hathaway, B.J., Billing, D.E., 1970. Coord. Chem. Rev. 5, 143.

Ibrahim, K.M., 1992. Mans. Sci. Bull. 19, 31.

Issa, I.M., Issa, M.R., Mahmoud, M.R., Temerk, Y.M.Z., 1973. Phys. Chem. 254, 314.

John, R.P., Sreekanth, A., Kurup, M.R.P., Usman, A., Ibrahim, A., Fun, H., 2003. Spectrochim. Acta 59A, 1349.

Kasumov, V.T., Köksal, F., Köseoğlu, R., 2004. J. Coord. Chem. 57, 591.

Khan, O., Mallah, T., Gouteron, J., Jeanin, S., Jeanin, Y., 1989. J. Chem. Soc., Dalton Trans., 1117.

Khasa, S., Seth, V.P., Gahlot, P.S., Agarwal, A., Krishna, R.M., Gupta, S.K., 2003. Phys. B 334, 347.

Khattab, M.A., Soliman, M.S., El-Enany, G., 1982. Bull. Soc. Chim. Belg. 91, 265.

Kumar, A., Prasad, R., Kociok-Köhn, G., Molloy, K.C., Singh, N., 2009. Inorg. Chem. Commun. 12, 686.

Lal, R.A., Choudhury, S., Ahmed, A., Chakraborty, M., Borthakur, R., Kumar, A., 2009. J. Coord. Chem. 62, 3864.

Llanguri, R., Morris, J.J., Stanley, W.C., Bell-Loncella, E.T., Turner, M., Boyko, W.J., Bessel, C.A., 2001. Inorg. Chim. Acta 315, 53.

Manoj, E., Prathapachandra Kurup, M.R., Punnoose, A., 2009. Spectrochim. Acta 72, 474.

Narang, K.K., Aggakwai, A., 1974. Inorg. Chim. Acta, 9137.

Perrin, D.D., 1976. In: Top. Curr. Chem., 181. Springer Verlag, New York.

Petering, H.G., Buskirk, H.H., Underwood, G.E., 1973. Cancer Res. 4, 367–372.

Pui, A., 2007. J. Coord. Chem. 60, 709.

Raman, N., Kulandalsamy, A., Thangaraja, C., 2003. Transition Met. Chem. 28, 29.

Sevagapandian, S., Rajagopal, G., Nehru, K., Athappan, P., 2000. Transition Met. Chem. 25, 388.

Sharma, S., Sharma, V., Bohra, R., Drake, J.E., Hursthouse, M.B., Light, M.E., 2007. Inorg. Chim. Acta 360, 2009.

Singh, N.K., Singh, S.B., 2001. Transition Met. Chem. 26, 487.

Syamal, A., Maurya, M.R., 1985. Ind. J. Chem. 24A, 836.

Thaker, B.T., Lekhadia, J., Patel, A., Thaker, P., 1994. Transition Met. Chem. 19, 623.

Thompson, L.R., Jeanette, D., Russell, B.P., Hitchings, H.G., 1953. Proc. Soc. Exp. Biol. Med. 84, 496.

Van Giessen, G.H., Crim, J.A., Petering, D.H., 1973. J. Nat. Cancer Inst. 51, 139.

Vogel, A.I., 1994. A Text Book of Quantitative Inorganic Analysis. Longmans, London.

Warad, D.U., Statish, C.D., Kulkarni, V.H., Bajgur, C.S., 2000. Ind. J. Chem. 39, 415.